CHAPTER IV

RESULTS AND DISCUSSION

4.1 Preparation and Characterization of Ligands

In the previous chapter, the preparative methods of ligands were described. The reactions employed in synthesis and structure identification of ligands will be discussed in this chapter. For many years, our group modifies *p-tert*-butylcalix [4]arene at the lower rim phenoxide moieties by attaching two ethoxybenzaldehyde groups *via* nucleophilic substitution reaction of *p-tert*-butylcalix[4]arene and 2-(2′-bromoethoxy)benzaldehyde or 2-(4′-bromoethoxy)benzaldehyde in the presence of base. The resulting dialdehyde *p-tert*-butylcalix[4]arene, **1** and **2**, are suitable for building macrocyclic or chelating frameworks for metal ion binding. Condensation reactions between the compounds **1** and **2** which contain aldehyde moieties and the dithia diamine compounds, 1,9-diaza-3,7-dithianonane and 1,8-diaza-3,6-dithiaoctane yielded four Schiff base ligands **3**, **4**, **5** and **6**, respectively. These reactions require high dilution conditions to prevent the formation of the polymeric products that may occur.[29] The ligands **3**, **4**, **5** and **6** precipitated out of the reaction mixtures in 85%, 71%, 43% and 40%, respectively. The yield of compounds **3** and **4** containing three carbons linkage between two nitrogen atoms is about twice as high as that of compounds **5** and **6** which contained two carbons linkage between two imine nitrogen atoms. This may be due to the fact that 1,8-diaza-3,6-dithiaoctane is more sensitive to moisture and air than 1,9-diaza-3,7-dithianonane. The *ortho*- substituted diaza dithiol compounds, **3** and **5**, can be obtained in 14% and 3% yield higher than the *para*-

substituted diaza dithiol compounds, **4** and **6**, respectively. This can be attributed to polymerization which simultaneously occurred with condensation reactions. *Ortho*-substited derivatives, **3** and **5**, should be less susceptible to polymerization than *para*-substited derivatives, **4** and **6**. According to low yield of compounds **5** and **6**, they were not used for further studies. Only compounds **3** and **4** were, therefore, subjected to pursue. Reduction of **3** and **4** was carried out by $NaBH_4$, and the reduced products were then protonated by a solution of HCl in methanol in order to produce more stable ammonium chloride derivatives, **7** and **8**, respectively. The preparative procedures of compounds **3** - **8** are depicted in Scheme 4.1.

Compounds **1–8** were characterized by ^1H NMR spectroscopy, IR spectroscopy, FAB MS and elemental analysis. All elemental analysis results agree with the propose structures of the compounds. ^1H NMR spectra of the Schiff base compounds **3**, **4**, **5** and **6** show characteristic singlet signals due to imine protons at 8.82, 8.19, 8.81 and 8.17 ppm, respectively. Upon reduction and hydrogenation of **3** and **4** to **7** and **8**, the imine signals disappear from the ^1H NMR spectra of **7** and **8** concurrent with signal broadening and appearance of the broad signals at 9.71 and 9.35 ppm which is a strong evidence for the positive charge at nitrogen atoms. ^1H NMR spectra of compounds **1–8** suggest that calix[4]arene compartments are in a cone conformation judging by two strong *tert*-butyl proton signals absorb at approximately 1.25 and 0.98 ppm and a doublet of doublet signal due to methylene bridge protons with a coupling constant of 13 Hz. IR spectra of both compounds **1** and **2** show strong bands due to carbonyl groups (>C=O) from aldehyde moieties at 1685 and 1695 cm^{-1}, respectively. In the other hand, IR spectra of compound **3**, **4**, **5** and **6** show bands due to C=N stretching at 1634, 1642, 1634 and 1640 cm^{-1}, respectively. FAB^+ mass spectra of compounds **3** and **4** show strong peaks at m/z 1103.1 and

1102.9, respectively agreeable with the molecular weight of proposed structures. However, FAB^+ mass spectra of compounds **7** and **8** show peak at m/z 1107.8 and 1108.2, respectively corresponding to the molecular mass of **7** and **8** when stripped off two molecules of hydrogen chloride.

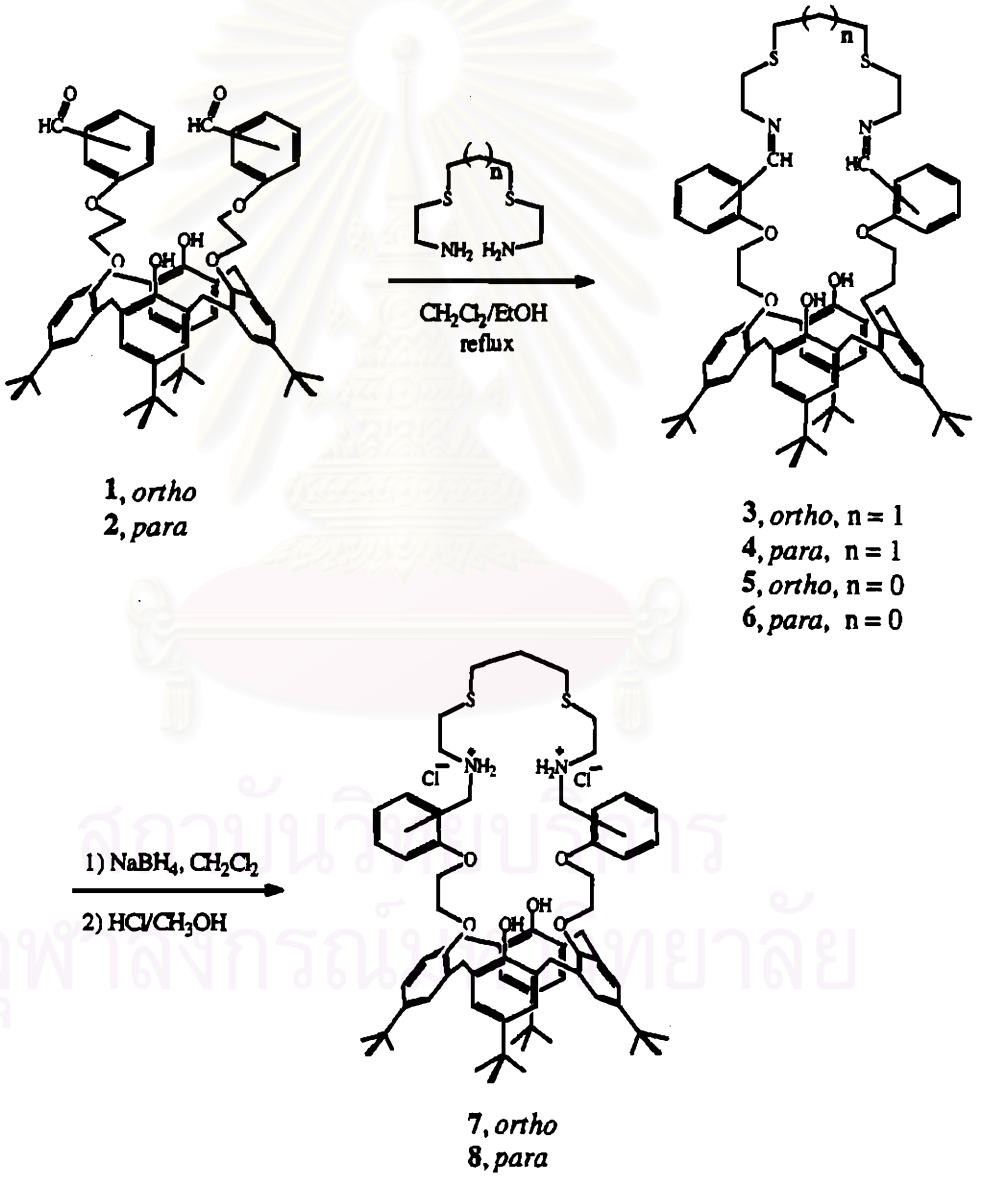

1, *ortho*
2, *para*

3, *ortho*, n = 1
4, *para*, n = 1
5, *ortho*, n = 0
6, *para*, n = 0

7, *ortho*
8, *para*

Scheme 4.1 Procedures for preparaion of compounds **3 – 8**.

4.2 Basicity and Complexation Studies

At least 40 points of potentiometric data were used in computer refinements to obtain protonation constants and complex stability constants which were calculated using the program **SUPERQUAD.**

4.2.1 Protonation Constants of Ligands

The two ligands 25,27-((2,2′-diethoxy)benzyl))-3,7-dithianonane-1,9-diamine-*p-tert*-butylcalix[4]arene dihydrogenchloride, **7**, and the 25,27-((4,4′-diethoxy)benzyl))-3,7-dithianonane-1,9-diamine-*p-tert*-butylcalix[4]arene dihydrogenchloride, **8**, were used for determination of the protonation constants. However, the results will be regarded as protonation constants of the two neutral compounds , 25,27-((2,2′-diethoxy)benzyl))-3,7-dithianonane-1,9-diamine-*p-tert*-butylcalix[4]arene, **9**, and the 25,27-((4,4′-diethoxy)benzyl))-3,7-dithianonane-1,9-diamine-*p-tert*-butylcalix[4]arene, **10**. Figure 4.1 shows the structures of compounds **9** and **10**.

The protonation constants of the compounds **9** and **10** in 10% CH_2Cl_2/CH_3OH (25 °C) using $1.0x10^{-2}$ M NMe_4Cl and $5.0x10^{-2}$ M $NBu_4CF_3SO_3$ as inert background electrolytes, are shown in Tables 4.1 and 4.2, respectively.

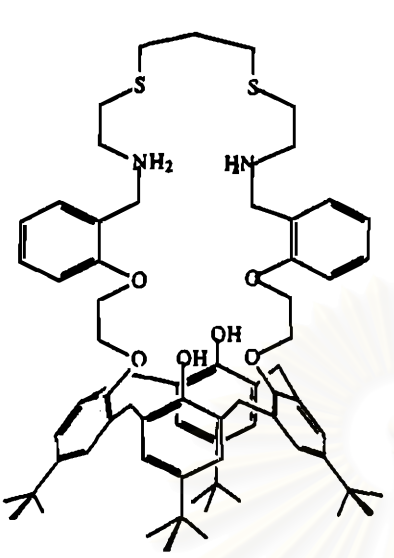

9

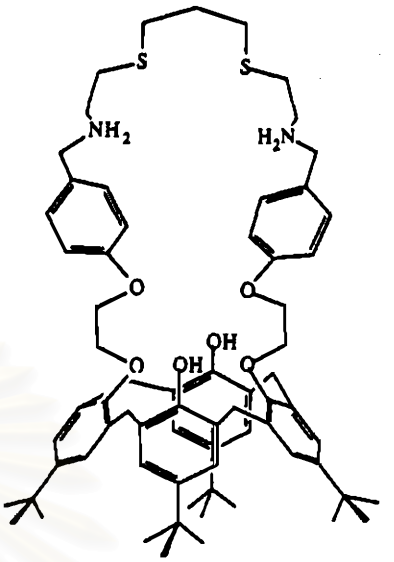

10

Figure 4.1 Structures of 25,27-((2,2′-diethoxy)benzyl))-3,7-dithianonane-1,9-diamine-*p*-*tert*-butylcalix[4]arene, **9**, and 25,27-((4,4′-diethoxy)benzyl))-3,7-dithianonane-1,9-diamine-*p*-*tert*-butylcalix[4]arene, **10**.

Table 4.1 Protonation constants of **9** and **10** in 10% CH_2Cl_2/CH_3OH (25 °C) using $1.0x10^{-2}$ M NMe_4Cl as electrolyte.

ligand	protonation		Log K
9	K_1 : L + H^+	LH^+	9.30 ± 0.04
	K_2 : LH^+ + H^+	LH_2^{2+}	9.23 ± 0.09
10	K_1 : L + H^+	LH^+	9.23 ± 0.05
	K_2 : LH^+ + H^+	LH_2^{2+}	7.82 ± 0.10

Table 4.2 Protonation constants of **9** and **10** in 10% CH_2Cl_2/CH_3OH (25 °C) using $5.0x10^{-2}$ M $NBu_4CF_3SO_3$ as electrolyte.

ligand	protonation		Log K
9	K_1 : L + H^+	LH^+	8.67 ± 0.01
	K_2 : LH^+ + H^+	LH_2^{2+}	7.82 ± 0.03
10	K_1 : L + H^+	LH^+	8.47 ± 0.02
	K_2 : LH^+ + H^+	LH_2^{2+}	7.87 ± 0.04

The titration curves of **9** and **10** in two inert background electrolytes at different initial concentrations are shown in Figures 4.2 and 4.3, respectively. The plots between $\bar{p}$ and log [H^+] for the ligands **9** and **10** in two inert background solutions are shown in Figures 4.4 and 4.5, respectively.

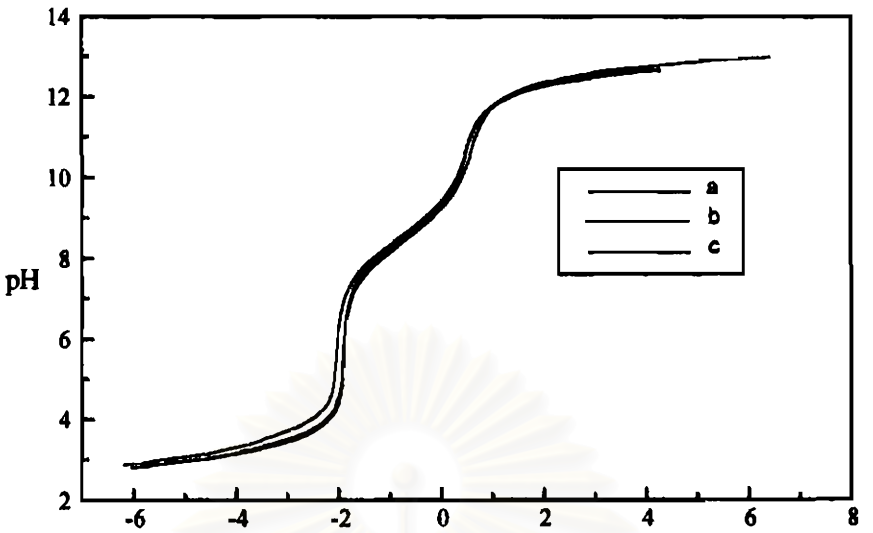

A

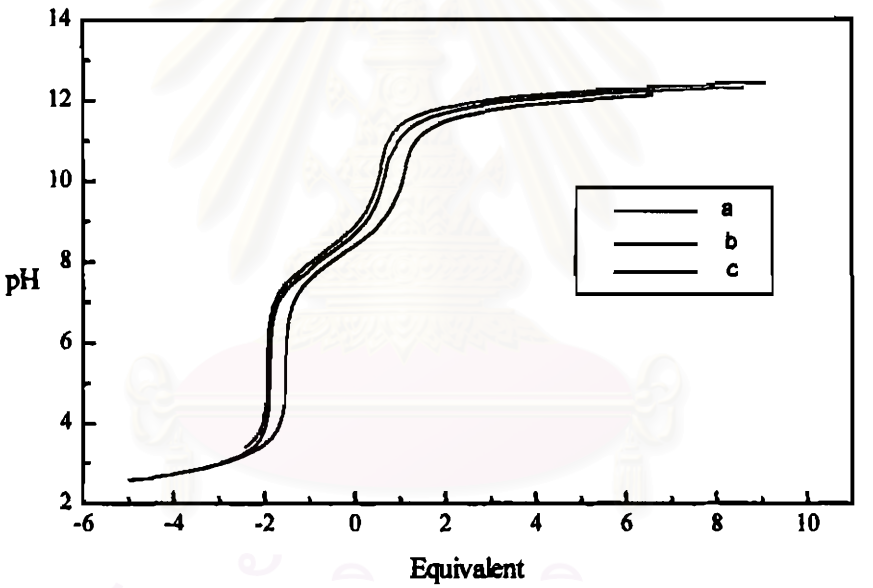

B

Figure 4.2 Potentiometric titration curves of **9** in 10% CH_2Cl_2/CH_3OH using **A)** $1.0x10^{-2}$ M NMe_4Cl as electrolyte at various ratio of **9** : proton : (a) 0.37 mM : 2.29 mM, (b) 0.34 mM : 2.10 mM and (c) 0.38 mM : 1.59 mM and **B)** $5.0x10^{-2}$ M $NBu_4CF_3SO_3$ as electrolyte at various ratio of **9** : proton : (a) 0.77 mM : 3.86 mM, (b) 0.91 mM : 2.74 mM and (c) 0.95 mM : 2.38 mM.

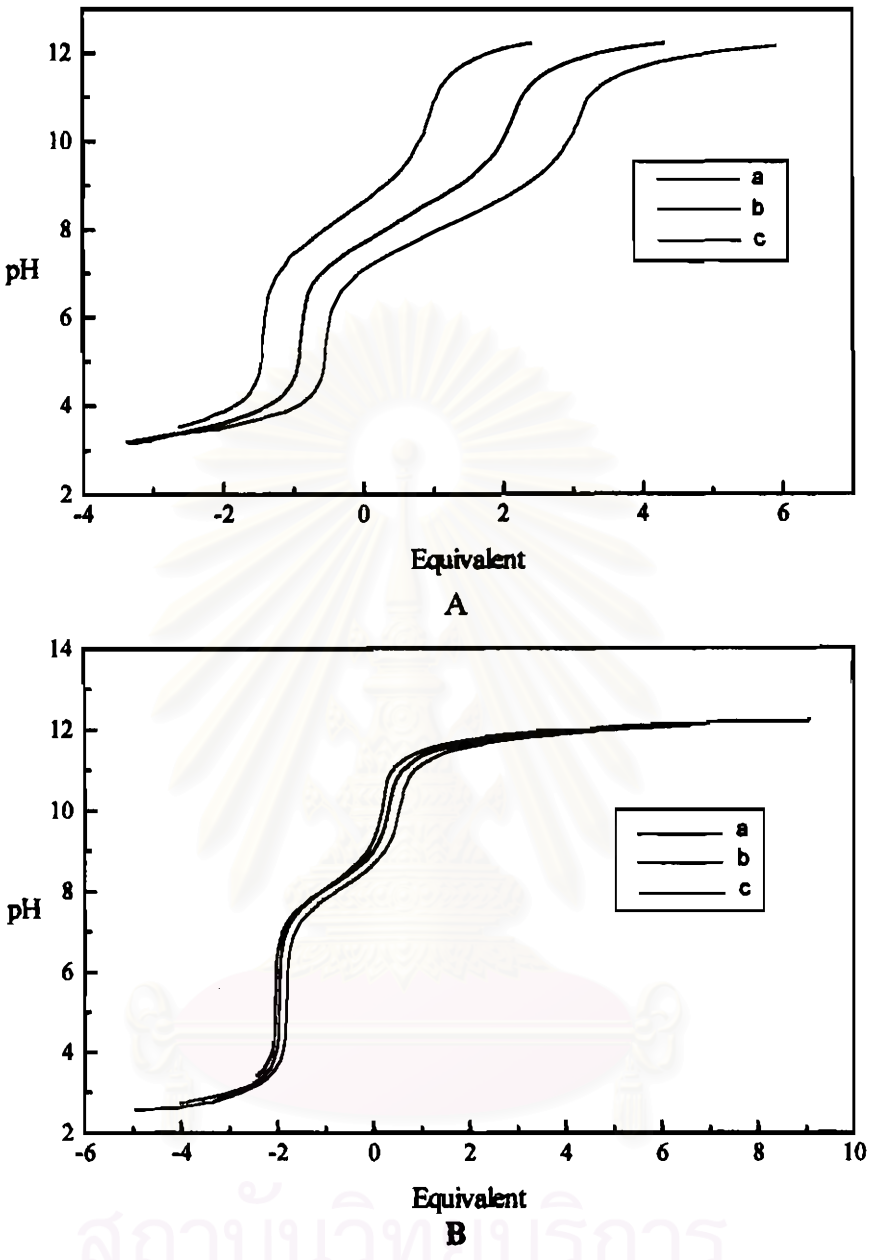

Figure 4.3 Potentiometric titration curves of **10** in 10% CH_2Cl_2/CH_3OH using **A)** $1.0x10^{-2}$ M NMe_4Cl as electrolyte at various ratio of **10** : proton : (a) 0.40 mM : 1.36 mM, (b) 0.40 mM : 1.36 mM and (c) 0.40 mM : 1.36 mM and **B)** $5.0x10^{-2}$ M $NBu_4CF_3SO_3$ as electrolyte at various ratio of **10** : proton : (a) 0.95 mM : 2.39 mM, (b) 0.83 mM : 3.34 mM and (c) 0.77 mM : 3.86 mM.

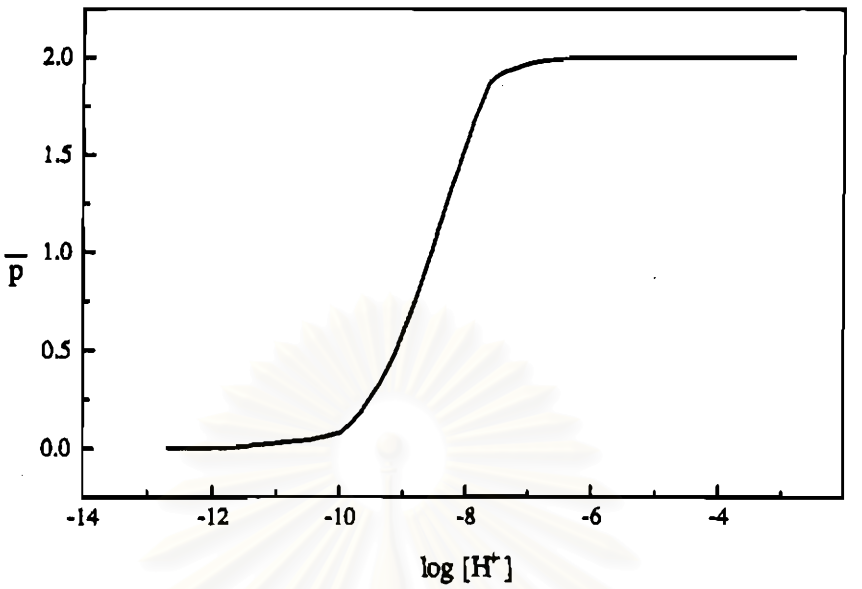

A

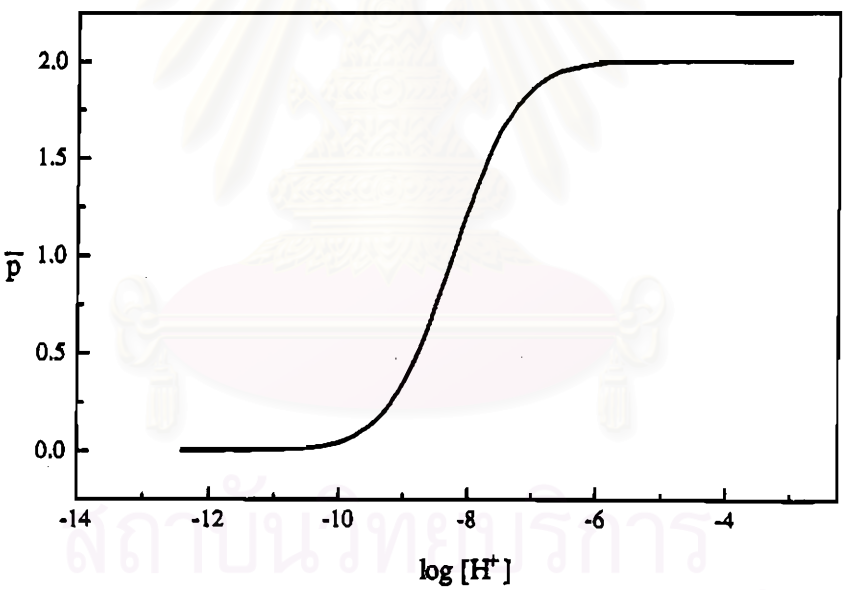

B

Figure 4.4 Plot between $\bar{p}$ and log [H^+] for **9** in 10% CH_2Cl_2/CH_3OH using **A)** 1.0 x10^{-2} M NMe_4Cl as electrolyte at various ratio of **9** : proton : 0.37 mM : 2.29 mM and **B)** 5.0x10^{-2} M $NBu_4CF_3SO_3$ as electrolyte at various ratio of **9** : proton : 0.77 mM : 3.86 mM.

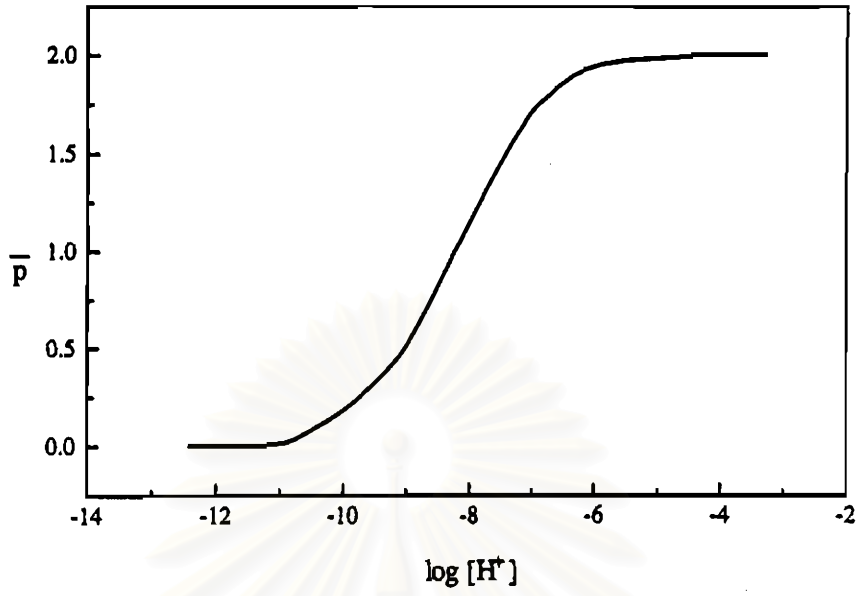

A

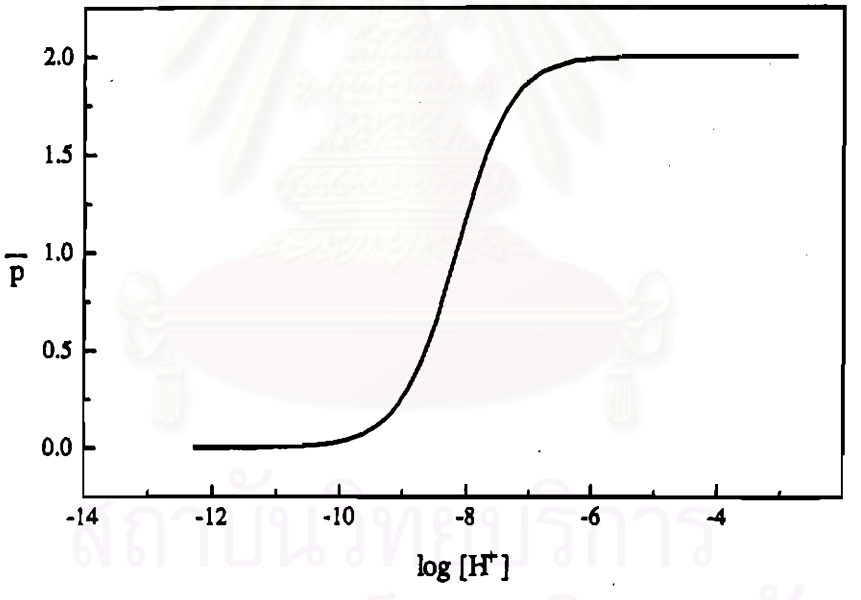

B

Figure 4.5 Plot between $\bar{p}$ and log [H^+] for **10** in 1 0% CH_2Cl_2/CH_3OH using **A)** 1.0 x10^{-2} M NMe_4Cl as electrolyte at various ratio of **10** : proton : 0.40 mM : 1.36 mM and **B)** 5.0x10^{-2} M $NBu_4CF_3SO_3$ as electrolyte at various ratio of **10** : proton : 0.95 mM : 2.39 mM.

According to the results in Tables 4.1 and 4.2, the first and second protonation constants of ligands **9** and **10** in $1.0x10^{-2}$ M NMe_4Cl and $5.0x10^{-2}$ M $NBu_4CF_3SO_3$ are comparable. The protonation constants indicate that these two ligands possess comparable basicity or donor ability. The first protonation constant of *ortho-* substituted *p-tert*-butylcalix[4]arene, **9**, is slightly bigger than that of *para-* substituted *p-tert*-butylcalix[4]arene, **10**, in the both inert background solutions. However, the second protonation constant of **9** is slightly smaller than that of **10**. These may be attributed to electronic effect of the substituted position. The ligand **9** has substituents at *ortho-* position, which may have more electrical effect (resonance and field) than *para-* position in **10**. Nitrogen atoms of **9** may, therefore, have more electron density than those of **10** resulting in better donor ability.[30] Both of nitrogen atoms of **9** are in *ortho-* position and are thus closer to each other than those in **10**. When the first nitrogen atom was protonated, the second nitrogen atom should be reluctant to receive the second proton because of the repulsion of positive charges. The second protonation constant of **10** is, therefore, a little higher than that in **9**.

According to Figures 4.4 and 4.5, all maximum values of $\bar{p}$ in every condition reach 2 which regard to the average number of protons bind to these ligands. Thus the results agree very well with structure of ligands **9** and **10** which have two amine-N atoms and can receive two protons in their structures.

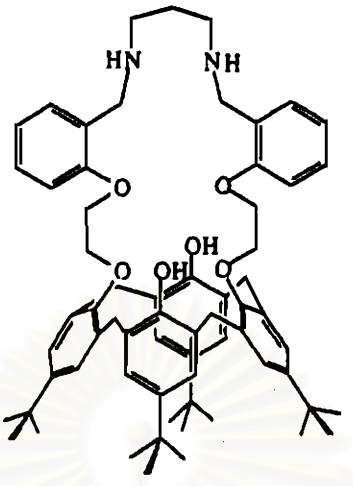

11

Figure 4.6 25,27-((2,2′-diethoxy)benzyl))-1,5-diamine-*p-tert*-butylcalix[4]arene.

Moreover, when compared the protonation constants of these ligands to the analogous compound **11**, the first protonation constant of compound **11** in methanol (log K_1 = 11.21±0.02) is a few number of magnitude higher than that of **9** and **10**. However the second protonation constant of **11** (log K_2 = 7.27±0.04) is comparable to those of **9** and **10**. Compound **11** was demonstrated by Vicens et al. to be a good extractant for Cu^{2+}, Pb^{2+}, Nd^{3+} and Eu^{3+}.[16]

The species distribution curves of **9** and **10** in 10% CH_2Cl_2/CH_3OH (25 °C) using two difference electrolytes, $1.0x10^{-2}$ M NMe_4Cl and $5.0x10^{-2}$ M $NBu_4CF_3SO_3$ are shown in Figures 4.7 and 4.8, respectively.

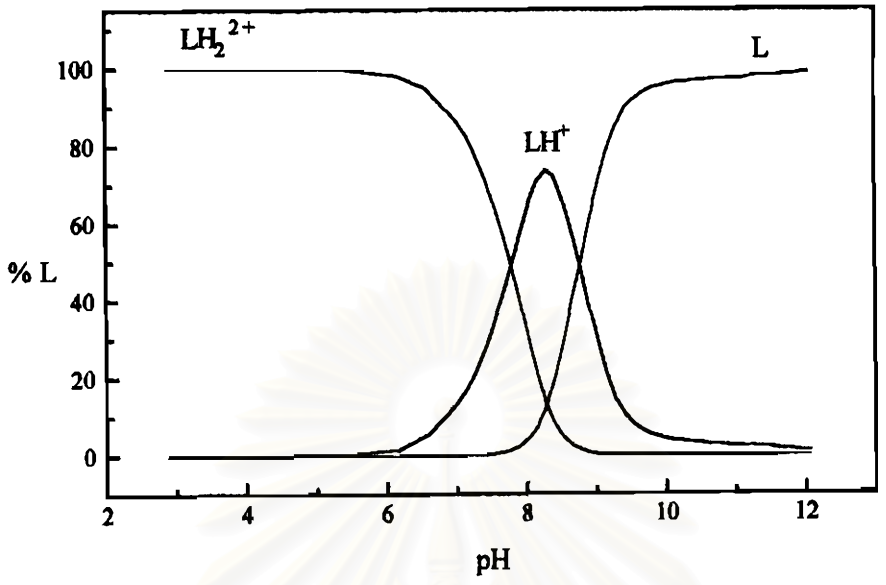

A

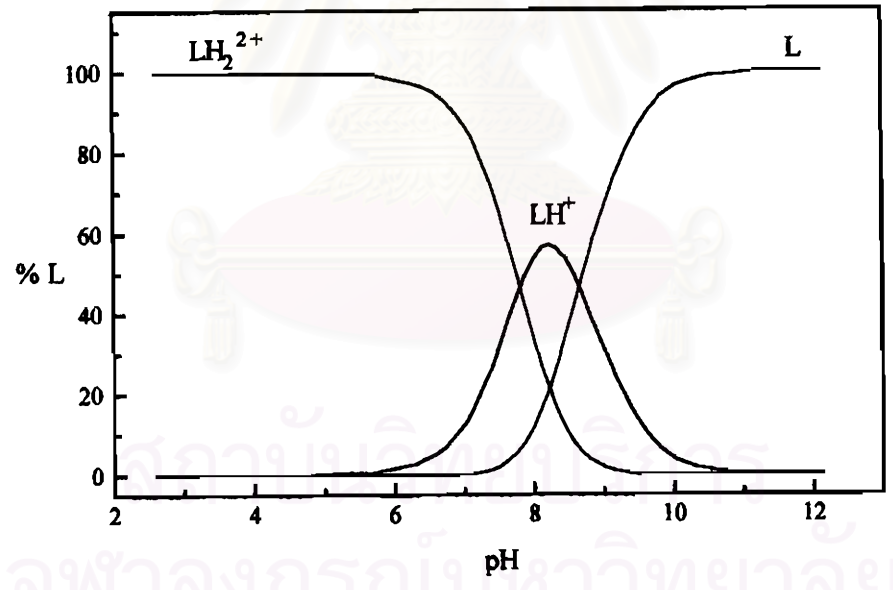

B

Figure 4.7 Species distribution curves of **9** in 10% CH_2Cl_2/CH_3OH using **A)** $1.0x10^{-2}$ M NMe_4Cl as electrolyte at 25 °C, C_L = 0.34 mM and **B)** $5.0x10^{-2}$ M $NBu_4CF_3SO_3$ as electrolyte at 25 °C, C_L = 0.77 mM.

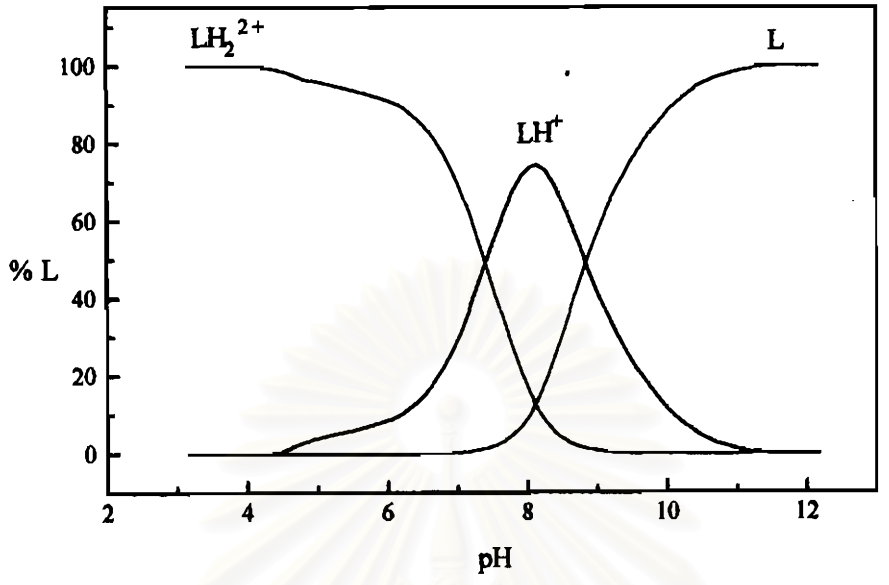

A

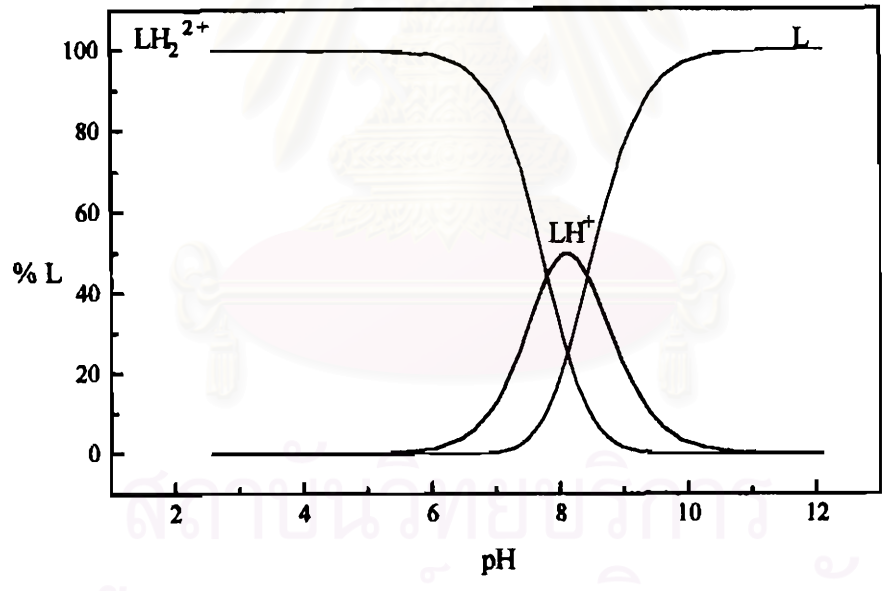

B

Figure 4.8 Species distribution curves of **10** in 10% CH_2Cl_2/CH_3OH using **A)** $1.0x10^{-2}$ M NMe_4Cl as electrolyte at 25 °C, C_L = 0.40 mM and **B)** $5.0x10^{-2}$ M $NBu_4CF_3SO_3$ as electrolyte at 25 °C, C_L = 0.77 mM.

In Figure 4.7, the species distribution plot of **9** in $1.0x10^{-2}$ M NMe_4Cl and in $5.0x10^{-2}$ M $NBu_4CF_3SO_3$ at 25 °C, shows that the LH_2^{2+} species is steeply decreased from 100% at pH 5.3 and 5.7, respectively to less than 5% at pH higher than 8.5 and 8.7, respectively. The LH^+ exists within the pH range of 5.3 to less than 5% at 9.8 and 5.7 to less than 5% at 10.0, respectively. The maximum percent of LH^+ species appears at pH 8.3 (74%) and pH 8.2 (57%) for NMe_4Cl and $NBu_4CF_3SO_3$ electrolytes, respectively. The **L** species exists at pH higher than 7.8 and 7.6 and its highest population is found at pH above 9.9 and 10.0, for NMe_4Cl and $NBu_4CF_3SO_3$, respectively.

In Figure 4.8, the species distribution plot of **10** in $1.0x10^{-2}$ M NMe_4Cl and in $5.0x10^{-2}$ M $NBu_4CF_3SO_3$ at 25 °C, shows that the LH_2^{2+} species is steeply decreased from 100% at pH 5.1 and 6.0, respectively to less than 5% at pH higher than 8.4 and 8.7, respectively. The LH^+ exists within the pH range of 5.2 to less than 5% at 10.5 and 5.7 to less than 5% at 10.0, respectively. The maximum percent of LH^+ species appears at pH 8.2 (74%) and pH 8.2 (50%) for NMe_4Cl and $NBu_4CF_3SO_3$ electrolytes, respectively. The **L** species exists at pH higher than 7.8 and 7.5 and its highest population is found at pH above 10.5 and 9.5 for NMe_4Cl and $NBu_4CF_3SO_3$, respectively.

4.2.2 Complexation of 25,27-((2,2′-diethoxy)benzyl)-3,7-dithianonane-1,9-diimine-*p*-*tert*-butylcalix[4]arene, 9, and 25,27-((4,4′-diethoxy)benzyl)-3,7-dithianonane-1,9-diimine-*p*-*tert*-butylcalix[4]arene, 10, with Cu^{2+}, Zn^{2+}, Cd^{2+} and Hg^{2+} ions

The ligands **9** and **10** possess soft donor S atoms and, therefore, were expected to form complexes with group IIB transition metal ions: Zn^{2+}, Cd^{2+} and Hg^{2+} ions, which are soft acids. We have also studied the complexation of **9** and **10** with Cu^{2+} ion which can form complexes in different geometries.

The studies were carried out by potentiometric titrations measuring concentration of each species versus pH that changed during experiments by addition of base. Stability constants of metal complexes of ligands **9** and **10** expressed in terms of logarithmic values (log β) are tabulated in Table 4.3.

Table 4.3 Stability constants of complexes of **9** and **10** towards Cu^{2+}, Zn^{2+}, Cd^{2+} and Hg^{2+} ions in 10% CH_2Cl_2/CH_3OH using $5.0x10^{-2}$ M $NBu_4CF_3SO_3$ as electrolyte at 25 °C.

ligand	Species of complexes	Log K			
		$M = Cu^{2+}$	$M = Zn^{2+}$	$M = Cd^{2+}$	$M = Hg^{2+}$
9	ML^{2+}	8.81 ± 0.04	-	-	4.47 ± 0.08
	$ML(OH)^{+}$	2.40 ± 0.07	-	-	-
	$ML(OH)_2$	-6.88 ± 0.15	-14.82 ± 0.09	-17.09 ± 0.13	-
10	ML^{2+}	7.21 ± 0.07	-	-	3.20 ± 0.13
	$ML(OH)^{+}$	1.64 ± 0.06	-	-	-
	$ML(OH)_2$	-8.64 ± 0.14	-15.54 ± 0.06	-16.80 ± 0.07	-

The titration curves of the complexes between the ligands **9** and **10** with Cu^{2+}, Zn^{2+}, Cd^{2+} and Hg^{2+} ions in 10% CH_2Cl_2/CH_3OH using $5.0x10^{-2}$ M $NBu_4CF_3SO_3$ as inert background electrolyte are shown in Figures 4.9, 4.10, 4.11 and 4.12 respectively. The plots of complex formation function, $\bar{n}$, of **9** and **10** with Cu^{2+} and Hg^{2+} versus the log [L] in 10% CH_2Cl_2/CH_3OH using $5.0x10^{-2}$ M $NBu_4CF_3SO_3$ as inert background electrolyte are shown in Figures 4.13 and 4.14, respectively.

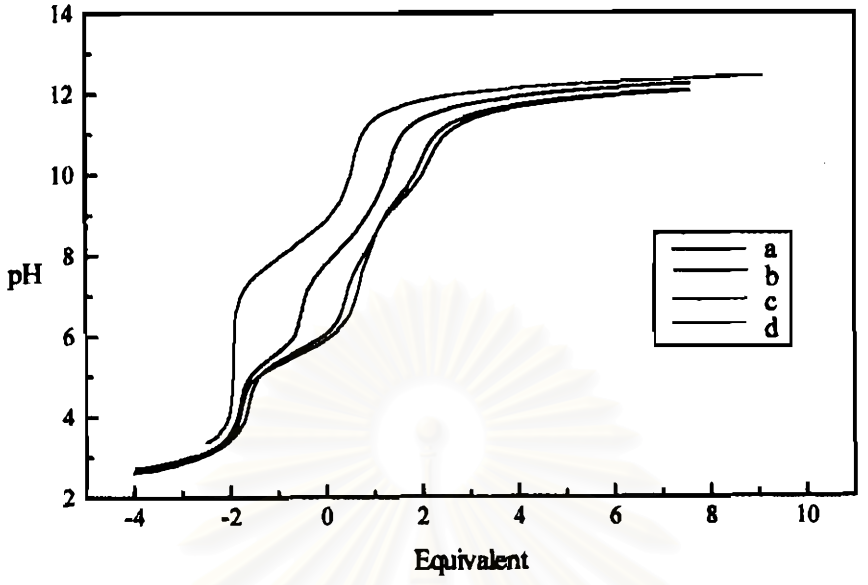

A

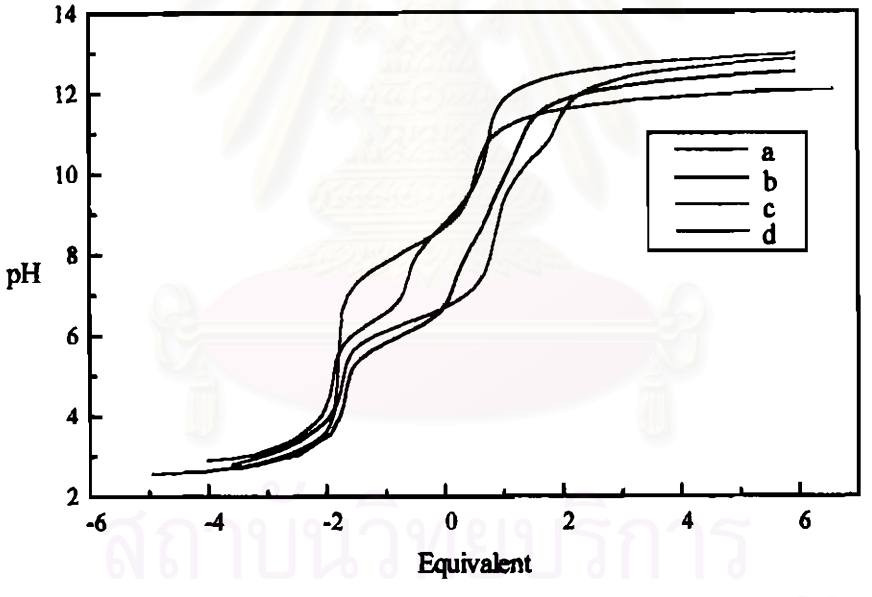

B

Figure 4.9 Potentiometric titration curves of **A)** ligand **9** with Cu^{2+} ion at various ratio of **9** : Cu^{2+} : (a) 0.95 mM : 0 mM, (b) 0.77 mM : 0.78 mM, (c) 0.80 mM : 0.40 mM and (d) 0.78 mM : 0.59 mM and **B)** ligand **10** with Cu^{2+} ion at various ratio of **10** : Cu^{2+} : (a) 0.83 mM : 0 mM, (b) 0.78 mM : 0.59 mM, (c) 0.77 mM : 0.78 mM and (d) 0.80 mM : 0.40 mM.

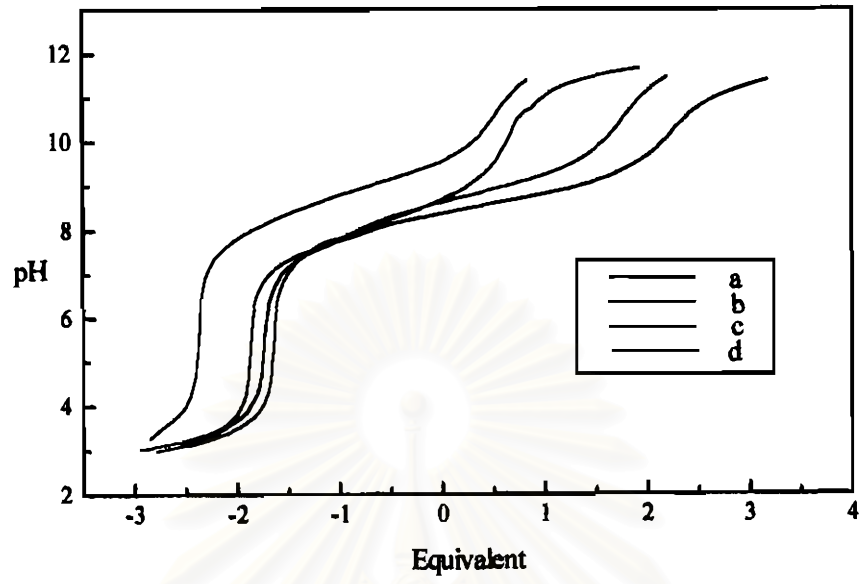

A

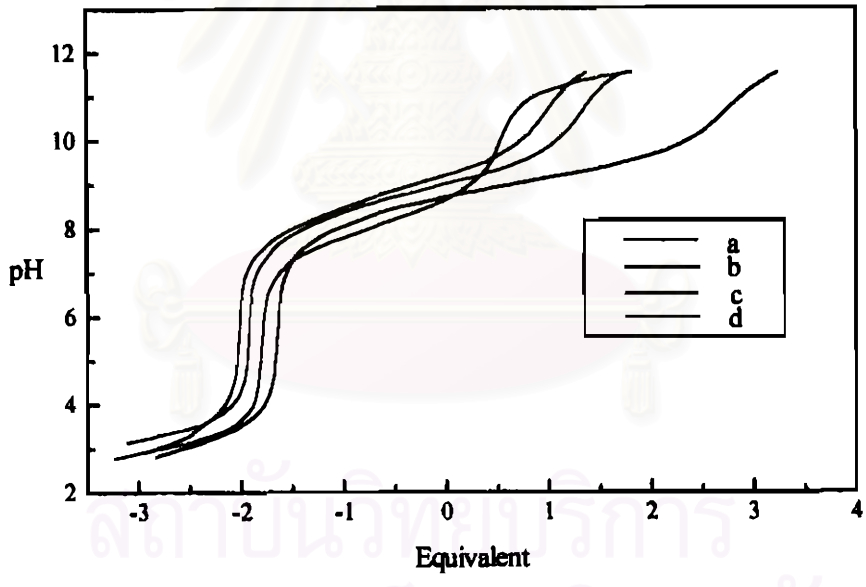

B

Figure 4.10 Potentiometric titration curves of **A)** ligand **9** with Zn^{2+} ion at various ratio of **9** : Zn^{2+} : (a) 0.95 mM : 0 mM, (b) 0.77 mM : 0.78 mM, (c) 0.79 mM : 0.59 mM and (d) 0.81 mM : 0.40 mM and **B)** ligand **10** with Zn^{2+} ion at various ratio of **9** : Zn^{2+} (a) 0.83 mM : 0 mM, (b) 0.78 mM : 0.78 mM, (c) 0.81 mM : 0.40 mM and (d) 0.78 mM : 0.59 mM.

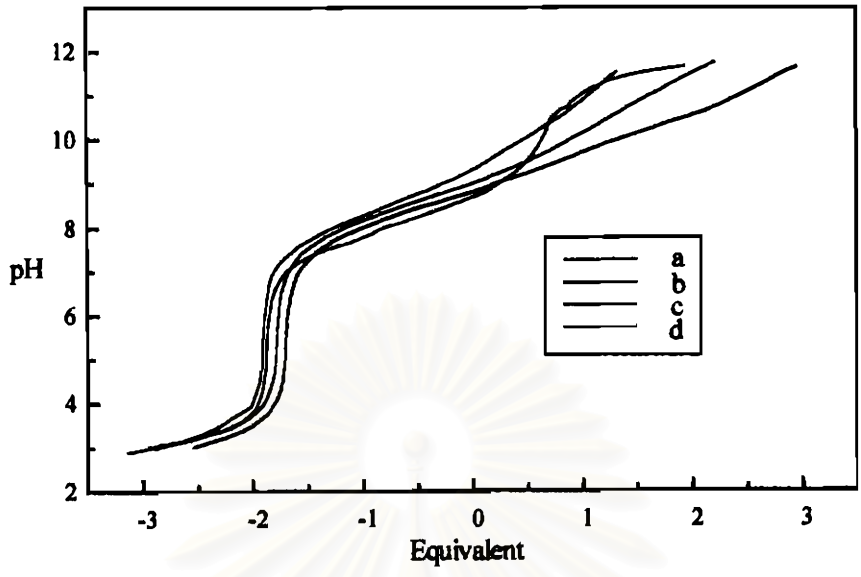

A

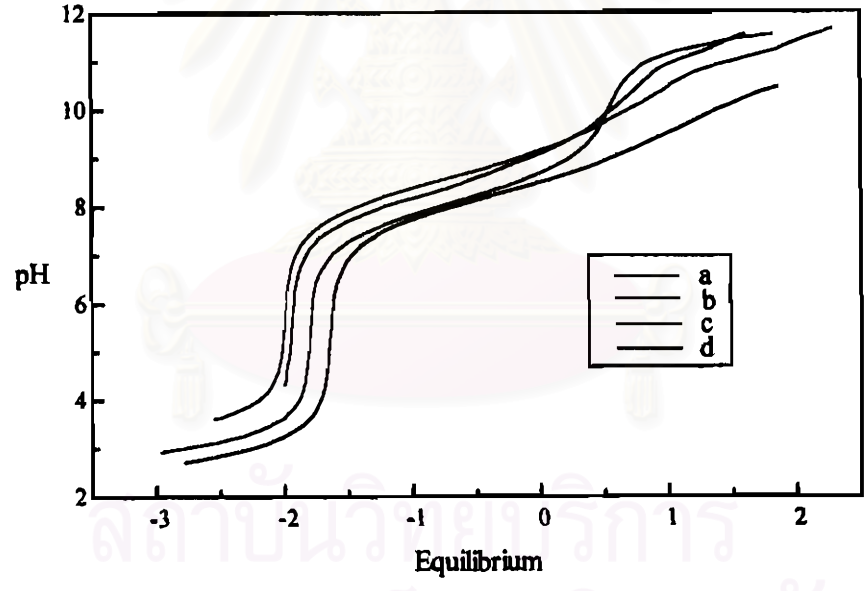

B

Figure 4.11 Potentiometric titration curves of **A)** ligand **9** with Cd^{2+} ion at various ratio of **9** : Cd^{2+} : (a) 0.95 mM : 0 mM, (b) 0.78 mM : 0.78 mM, (c) 0.81 mM : 0.41 mM and (d) 0.79 mM : 0.60 mM and **B)** ligand **10** with Cd^{2+} ion at various ratio of **10** : Cd^{2+} : (a) 0.83 mM : 0 mM, (b) 0.78 mM : 0.59 mM, (c) 0.77 mM : 0.78 mM and (d) 0.80 mM : 0.40 mM.

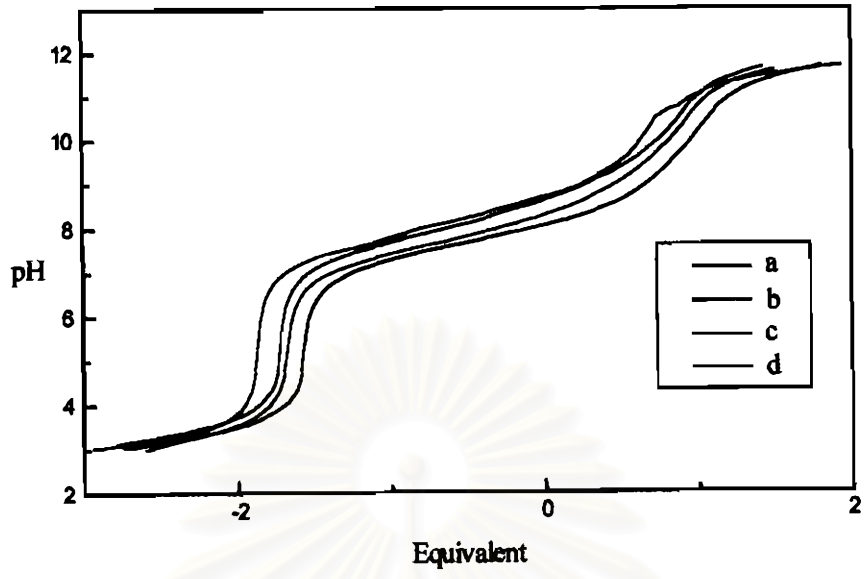

A

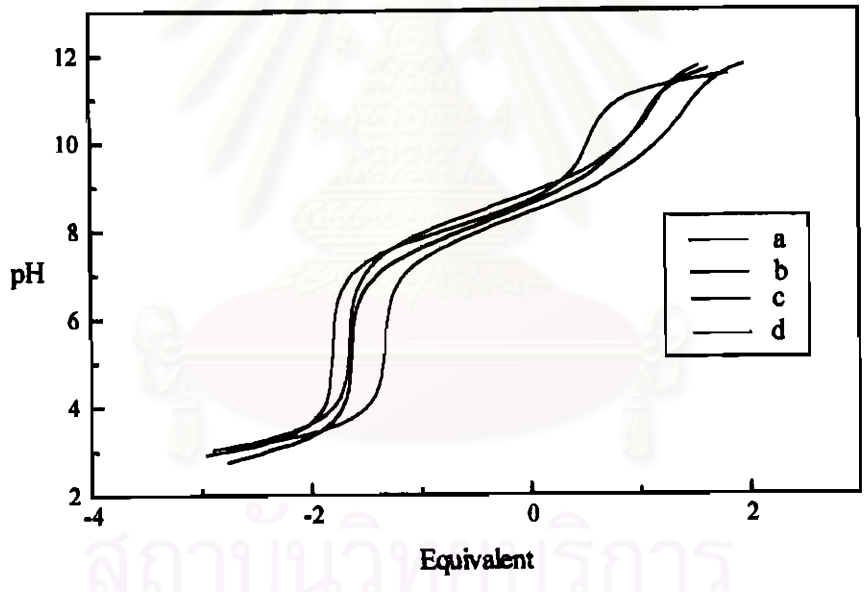

B

Figure 4.12 Potentiometric titration curves of **A)** ligand **9** with Hg^{2+} ion at various ratio of **9** : Hg^{2+} : (a) 0.95 mM : 0 mM, (b) 0.78 mM : 0.78 mM, (c) 0.81 mM : 0.41 mM and (d) 0.79 mM : 0.60 mM and **B)** ligand **10** with Hg^{2+} ion at various ratio of **10** : Hg^{2+} : (a) 0.83 mM : 0 mM, (b) 0.78 mM : 0.59 mM, (c) 0.77 mM : 0.78 mM and (d) 0.80 mM : 0.40 mM.

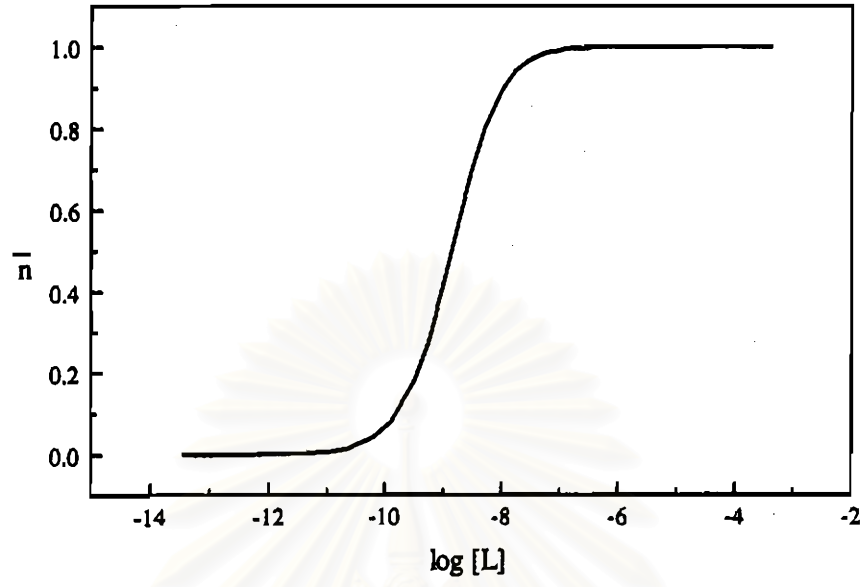

A

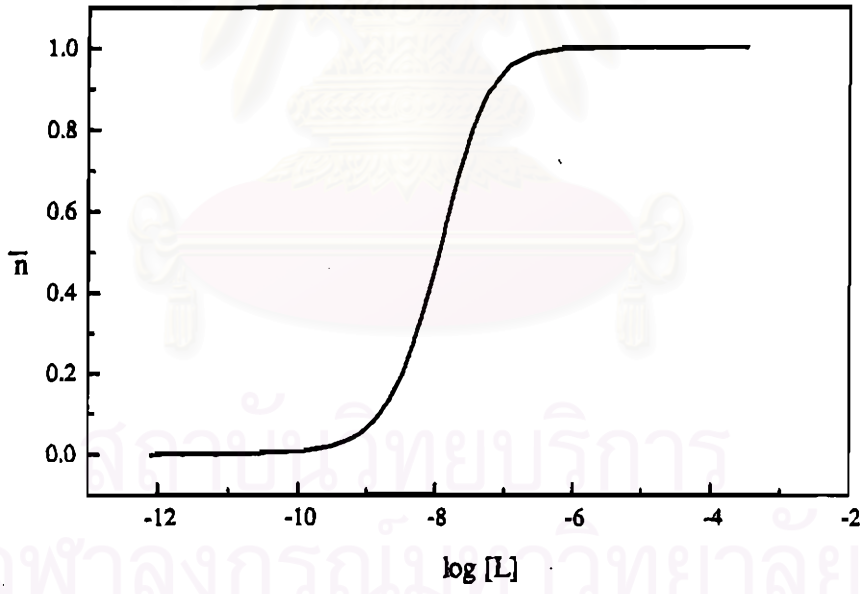

B

Figure 4.13 Plot between $\bar{n}$ and log [L] for Cu^{2+} complexes with **A)** ligand **9** at the concentration ratio (**9** : Cu^{2+}) of 0.80 mM : 0.40 mM and **B)** ligand **10** at the concentration ratio (**10** : Cu^{2+}) of 0.77 mM : 0.78 mM.

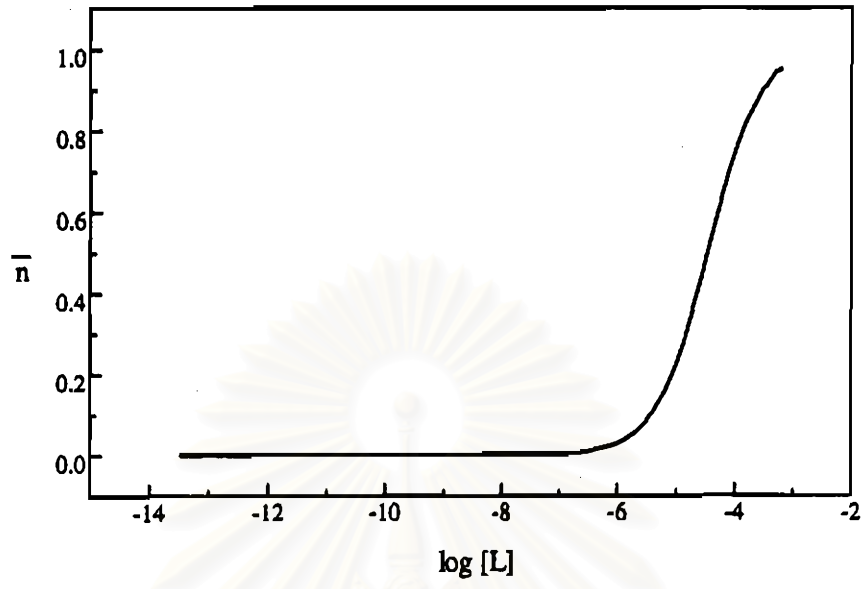

A

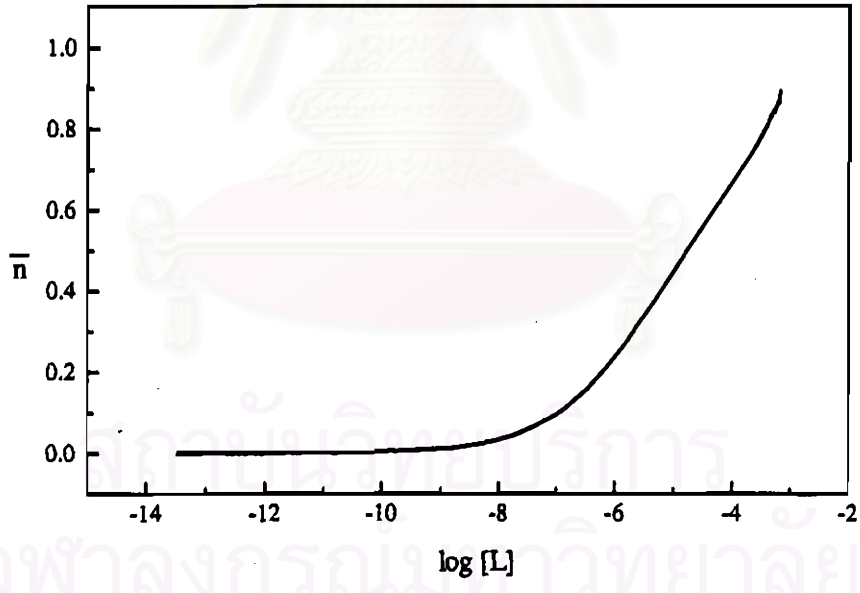

B

Figure 4.14 Plot between $\bar{n}$ and log [L] for Hg^{2+} complexes with **A)** ligand **9** at the concentration ratio (**9** : Hg^{2+}) of 0.80 mM : 0.40 mM and **B)** ligand **10** at the concentration ratio (**10** : Hg^{2+}) of 0.77 mM : 0.78 mM.

According to Table 4.3 and Figures 4.9, 4.10, 4.11, 4.12, 4.13 and 4.14, the results show that ligands **9** and **10** do not form 1:1 complexes (ML^{2+}) with Zn^{2+} and Cd^{2+} ions at all. However, both **9** and **10** form hydroxide complexes with Zn^{2+} and Cd^{2+}, i.e. $ZnL(OH)_2$ and $CdL(OH)_2$, respectively with low stability constants. These values are insignificant. We can thus state that the ligands **9** and **10** do not form the complexes with Zn^{2+} and Cd^{2+}.

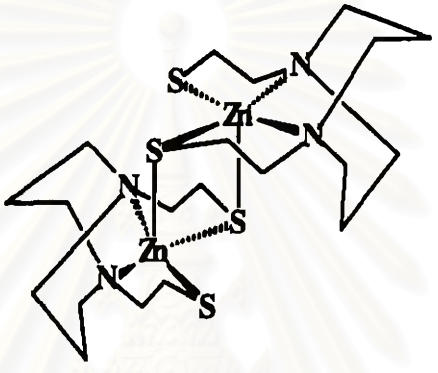

Figure 4.15 $(Znbme\text{-}daco)_2$ complex, **12**

Considering the most preferable geometry of Zn^{2+} and Cd^{2+} complexes, tetrahedral geometry, we think that our ligand environments are not suitable for forming complexes with these ions. The N_2S_2 donor set of **9** and **10** inclines to coordinate metal ions in a square planar fashion. Nevertheless, six coordinate octahedral geometry may occur since the metal can use the N_2S_2 donor set of **9** and **10** as equatorial ligands and two OH^- ions as axial ligands. The ethylene and propylene pendant arms of both ligands may be too strained to rearrange themselves to support tetrahedral geometry. A ligand, *N,N'*-bismercaptoethyl-1,5-diazacyclooctane (bme-daco), prepared by Darenbourg and coworkers has a similar donor set to ligands **9** and **10**,[31] and was found to react with $Zn(acac)_2$ to give a binuclear square pyramidal complex $(Znbme\text{-}daco)_2$, **12** (Figure 4.15), as a product rather than a mononuclear tetrahedral complex due to ligand constraint.[32]

The complexation studies of ligands **9** and **10** with Cu^{2+} can probe this hypothesis. They can give a square planar complex for a ligand that has N_2S_2 donor set.[33] The results in Table 4.3 and Figures 4.13 and 4.14 show that both **9** and **10** indeed form 1:1 CuL^{2+} complexes with stability constants (log K's) of 8.81±0.04 and 7.21±0.07 respectively. Besides, $CuL(OH)^{+}$ and $CuL(OH)_2$ complexes were also found in complexation studies probably due to versatile coordination chemistry of Cu^{2+} ion.[34]

The ligands **9** and **10** form 1:1 complexes with Hg^{2+} ions with stability constant values of 4.47±0.08 and 3.20±0.13, respectively. It has been long known that Hg^{2+} complexes have stability constant higher than that of Zn^{2+} and Cd^{2+} ions.[35,36] However, Hg^{2+} can bind to a sulfur-donor ligand and give a linear two-coordinate metal complex as demonstrated by Hosseini et. al. who have found that *p-tert*-butyltetramercaptocalix[4]arene can form a complex with Hg^{2+} by linear S-coordinations.[18,19]

In addition to stability constants, potentiometric titration can give more information of the behavior of metals and ligands in solution. A species distribution plot is a good source of such information. The species distribution curves of the complexes of **9** and **10** with Cu^{2+} and Hg^{2+} in 10% CH_2Cl_2/CH_3OH using $5.0x10^{-2}$ M $NBu_4CF_3SO_3$ computed from their stability constants and titration data are shown in Figures 4.16 and 4.17, respectively.

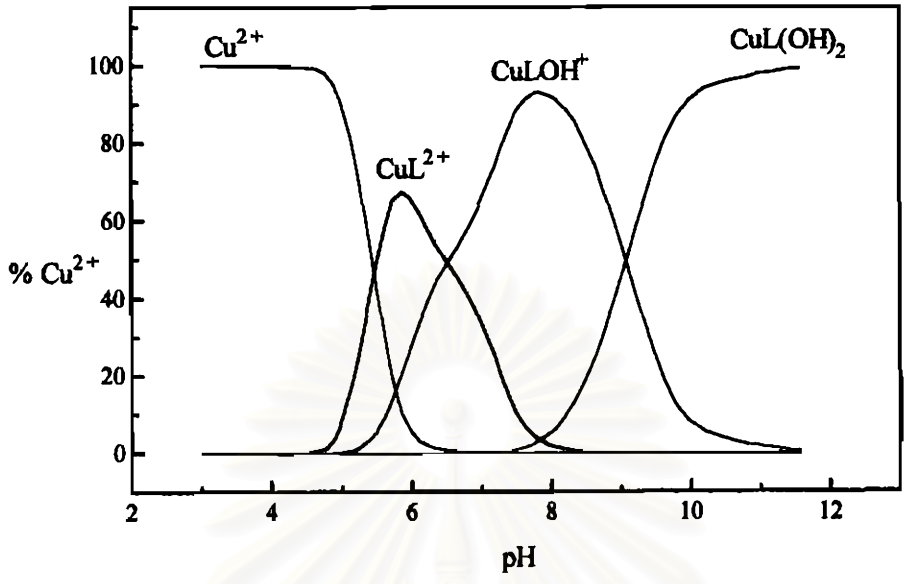

A

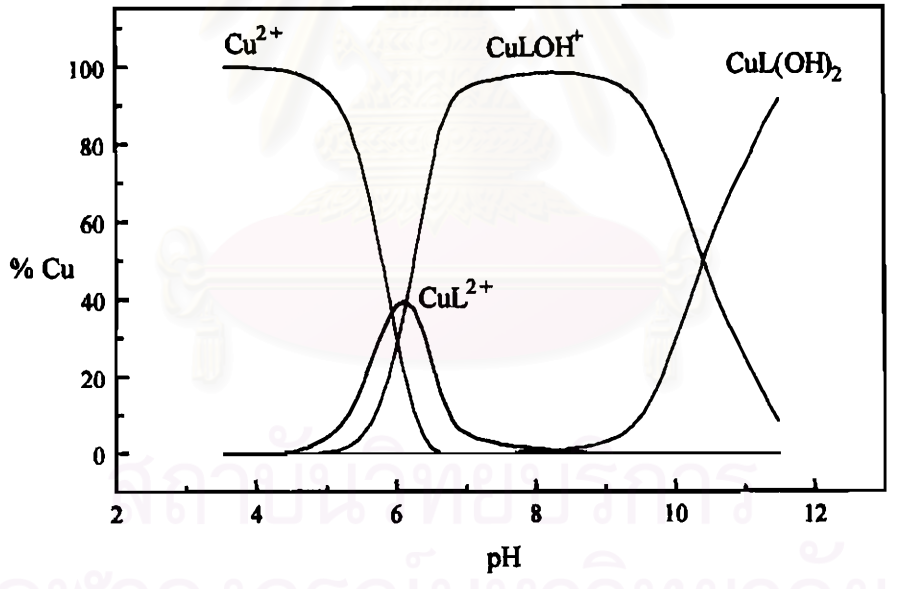

B

Figure 4.16 Species distribution curves of the Cu^{2+} complexes in 10% CH_2Cl_2/CH_3OH using $5.0x10^{-2}$ M $NBu_4CF_3SO_3$ as electrolyte at 25°C **A)** for **9** at the concentration ratio (**9** : Cu^{2+}) of 0.40 mM : 0.80 mM and **B)** for **10** at the concentration ratio (**10** : Cu^{2+}) of 0.59 mM : 0.78 mM.

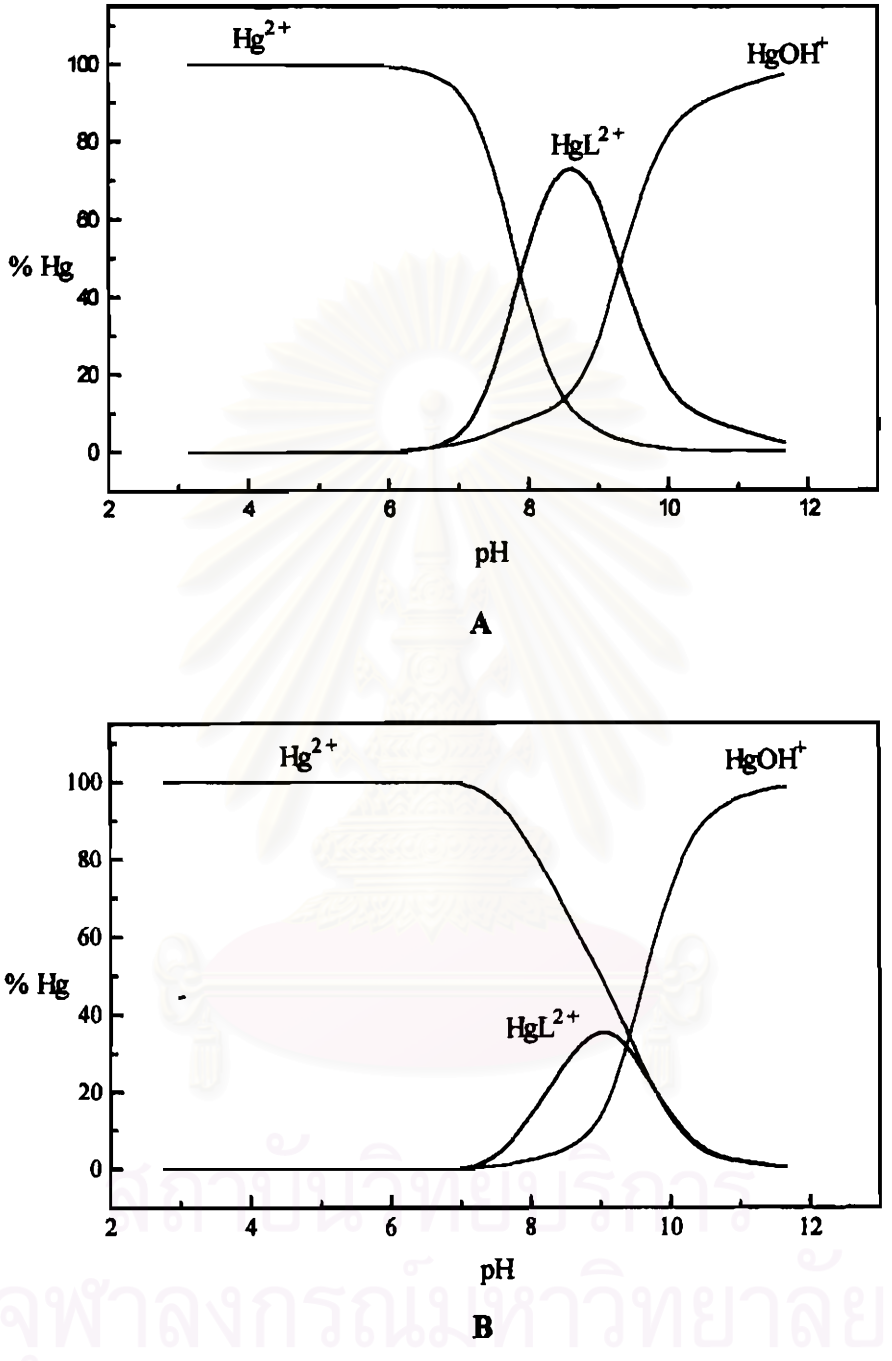

Figure 4.17 Species distribution curves of the Hg^{2+} complexes in 10% CH_2Cl_2/CH_3OH using $5.0x10^{-2}$ M $NBu_4CF_3SO_3$ as electrolyte at 25°C **A)** for **9** at the concentration ratio (**9** : Hg^{2+}) of 0.39 mM : 0.78 mM and **B)** for **10** at the concentration ratio (**10** : Hg^{2+}) of 0.39 mM : 0.78 mM.

According to Figure 4.16, for Cu^{2+}, the ligand **9** and **10** form the highest amount of 1:1 complexes with Cu^{2+} at pH 5.9 (68%) and at pH 6.2 (40%), respectively. The CuL^{2+} complexes exist within the pH range of 4.9 to 7.7 and 5.1 to 7.1 for ligands **9** and **10**, respectively. In case of Hg^{2+}, the highest amount of 1:1 complexes with **9** and **10** occurred at pH 8.7 (73%) and at pH 9.1 (36%), respectively. Figure 4.17 shows that the HgL^{2+} complexes exist within the pH range of 7.0 to 9.1 and 7.5 to 10.5 for ligands **9** and **10**, respectively. Only Cu^{2+} ion forms $ML(OH)^{+}$ and $ML(OH)_2$ species. The $CuL(OH)^{+}$ complexes exist within the pH range 5.4 to 10.3 and 5.5 to 11.6 for ligands **9** and **10**, respectively. The $CuL(OH)_2$ complexes exist at pH 7.9 and at pH 9.3 for ligands **9** and **10**, respectively.